CONF-860605--33

CONF-860605--33

DE87 001426

VOID-PRECIPITATE ASSOCIATION DURING NEUTRON IRRADIATION OF AUSTENITIC STAINLESS STEEL*

D. F. Pedraza and P. J. Maziasz

Metals and Ceramics Division, Oak Ridge National Laboratory,
P. O. Box X, Oak Ridge, TN 37831 (USA)

ABSTRACT: Microstructural data has recently become available on a single heat of 316 stainless steel irradiated in EBR-II and HFIR, over a wide range of irradiation temperature (55 to 750 C), dose (7 to 75 dpa), and helium generation rate (0.5 to 55 at. ppm He/dpa). Extensive information on precipitate compositions and characteristics are included. The data reveal several important relationships between the development of voids and precipitation. Precipitate associated voids dominate the swelling of (DO heat) 316 at 500–650 C from 8.4 to 36 dpa in EBR-II. Cold work (CW) or helium preinjection delay void formation in EBR-II. Higher helium generation in HFIR also delays void formation at 500–640°C in SA and CW DO heat 316. The delay persists in CW 316 at least to 61 dpa in HFIR, but abundant matrix and precipitate-associated voids form in SA 316 after 47 dpa. In another heat of CW 316 (N-lot) irradiated in HFIR matrix and precipitate voids form readily after 22–44 dpa at 500–600°C. Precipitate-associated void formation is intimately connected to phase nature, and to details of

---

*Research sponsored by the Division of Materials Sciences and Office of Fusion Energy, U.S. Department of Energy, under contract DE-AC05-84OR21400 with Martin Marietta Energy Systems, Inc.

dislocation and bubble evolution. Analysis of this data suggests a mechanism which relates to the origin and subsequent growth of precipitate associated voids.

KEY WORDS: Swelling, Neutron Irradiation, Austenitic Stainless Steels, Microstructure, Phase Stability, Radiation Induced Segregation, Voids, Precipitation, Helium Effects

INTRODUCTION

Large voids directly associated with precipitate phase particles have been a prominent feature of the microstructure of neutron irradiated stainless steels since the discovery of voids nearly 20 years ago [1]. However, that association did not receive much experimental or theoretical attention until recently [2–8]. Some investigators did single out the phenomenon [9,10] and proposed [9,11] possible mechanisms that would enhance void formation and growth at a precipitate/matrix interface. Brager and Straalsund [9] suggested that helium and vacancies preferentially accumulate to particular interfaces to assist void evolution. Brailsford and Bullough [11] proposed that an incoherent precipitate interface favors void formation because it is a non-saturable point defect sink. Conversely, a coherent precipitate can retain point defects, with a saturable capacity, until annihilation occurs by recombination with arriving anti-defects. More recently, Mansur [3] developed a quantitative model of precipitate-attached void growth enhancement relative to matrix (free) voids based on a point defect collector mechanism acting over the entire precipitate interface. He included a method to account for differences in point defect capture efficiencies by different precipitates in order to explain why voids grow at diffrent rates when attached to different precipitates. Odette and Stoller [7] have evaluated the transition from gas driven to bias driven regimes in terms of a critical radius concept, including sensitivities to oversized or undersized precipitate misfit

strains and overall microstructural evolution. Recent experimental observations [7,8,12,13] suggest a complex relationship of void formation to phase nature and total microstructural evolution.

From about 1964–1972, precipitation in neutron irradiated steels was primarily thought to be an irradiation enhanced thermal phenomenon [14–16]. From 1972–1978, the discovery of many irradiation induced [9,17,18] and/or nickel and silicon rich phases [19,20], suggested that precipitation under irradiation may be quite different from that occurring under thermal aging. Only after 1979 has the full picture of precipitation under irradiation begun to emerge with the development of modern analytical electron microscopy (AEM). Precipitation in steels was shown to include several classes of phases [21–24]. Thermal phases can be either enhanced or retarded by irradiation with little or no compositional change. Thermal phases that undergo compositional changes during irradiation are classed as modified phases. Finally radiation induced phases do not form during very long aging (~10,000 h) in that particular alloy and dissolve during post-irradiation annealing. Such phases can precipitate, however, during aging if the bulk alloy composition is appropriately changed, as demonstrated by Williams, et al. [25,26].

Helium generation is a very important element of the primary damage to be produced in fusion reactors because of its high level. Helium has been shown to enhance or retard void formation and to influence the precipitation pattern under irradiation and under aging [8,13]. These changes in the relative evolution of the various microstructural components at higher

helium levels provide additional insight into their interrelationship at lower helium levels.

The purpose of this work is to present an overall characterization of precipitate-void association (PVA) in two heats of neutron irradiated austenitic stainless steels in the context of the overall microstructural evolution, and to develop some ideas relating to possible mechanistic explanations. First, an overview of experimental observations is presented. More details have been [8,12,27–30] or will be presented elsewhere. Many specimens are from a single heat (DO) of type 316 stainless steel. The samples were irradiated in the solution annealed and 20% cold worked conditions in two reactors — EBR-II and HFIR — at various temperatures and fluences. Additional SA and CW specimens were irradiated in EBR-II after helium preinjection. Specimens of a different heat of type 316, N-lot, was also irradiated in HFIR in the 20% CW condition. The comparison of results on both heats permits us to point out differences as well as to emphasize general trends in the microstructural development. The compositions are presented in Table I. Specific characteristics of the precipitates are described in order to single out those that correlate with the occurrence of either PVA or matrix (precipitate-free) voids. Finally, from the analysis of experimental observations we suggest a mechanism that relates to the origin and subsequent growth of precipitate-associated voids.

GENERAL SURVEY OF MICROSTRUCTURAL RESULTS

Void formation in the context of overall microstructural evolution will be the focus of this section, with emphasis on precipitate-associated void development. We attempt to consistently distinguish between bubbles

and voids in the matrix based on a suggested system of relative size comparison to the bubbles found along grain boundaries in the same specimen [12]. We first survey the experimental data on SA-316 irradiated in EBR-II, where the highest void swelling is observed. Next, we describe the sensitivity of void formation to material conditions (e.g., helium preinjection, cold work) and/or reactor damage parameters (temperature, fluence, helium generation rate).

EBR-II Irradiations

SA (DO-heat) 316 — Nearly all the voids are directly attached to precipitate particles after 8.4 dpa at 500 and 625 C (see Table II and Figure 1). As dose is increased to 31—36 dpa, the swelling increases and is mostly due to precipitate associated voids at both temperatures (Fig. 2). At 625 C both the precipitates and their associated voids increase in size with dose while their number density decreases slightly. However, at ~525 C voids become much more abundant with little additional growth. In either case, precipitate associated voids are 2—3 times larger than matrix voids (Table 2). Most voids are attached to $M_6C(\eta)$ particles in this temperature range. However, at 630 C and 36 dpa, voids are equally distributed between η and Laves particles which are present in equal proportions (Figs. 2b, 3a and 3b).

Various radiation induced phases are present at low dose, coexisting with Frank (faulted) loops. G, γ' (Ni_3Si) and many needle-shaped phosphides (M_2P and/or M_3P types) are present at 500 C, whereas only needle

phosphides are found at 625 C. Nearly all G-phase particles and some of the phosphide needles are attached to voids (Figs. 3c and 3d), but the γ' particles are void free. As fluence increases, loops and the irradiation induced phases disappear from the microstructure, except at 525 C where a small amount of phosphide needles remains after 31 dpa.

In contrast to the instability of the radiation induced phases, the abundance of coarse η and/or Laves, which are radiation modified or enhanced, increases with dose up to 31–36 dpa. Precipitate volume fractions are shown at 500–525 C in Fig. 4a. A few matrix voids develop after 31 dpa, even though a high density of fine bubbles also appear which were not observed at low fluence.

Relative to observations on many other heats of SA 316 irradiated in EBR-II [9,10,31–35], this DO heat has far fewer total voids, but a larger fraction of precipitate associated voids. The other heats of steel have, in general, many more loops and higher dislocation concentrations. It is more difficult to assess differences in precipitation under irradiation because phase identification was often uncertain prior to 1978–80.

CW (DO-heat) 316 — Cold working by ~20% raises the dislocation network concentration of unirradiated specimens by a factor of $\sim 10^4$ relative to solution annealed material. This causes the microstructural evolution of CW 316 to differ significantly from that of SA 316 after low and medium fluence irradiations in EBR-II. Void formation at 500 and 630 C is delayed until around 30 dpa (see Table III and Fig. 5.) Voids develop in patches

after 36 dpa. Larger voids attached to η and Laves are similar to those found in SA 316, but the CW 316 has many more matrix voids. Above 36 dpa, the void size and number density increase substantially at 500 and 630 C. After 69 dpa at 510 C their size has doubled and their number density has increased ~20 times. Most voids that formed in the matrix between faulted bands are connected to several smaller G and Laves precipitates, whereas along faulted bands they are attached to larger η particles. After 75 dpa at 620 C, the matrix voids are much more abundant than those attached to precipitates and they have grown to a similar size as seen at the lower temperature. Precipitate particles and their associated voids have coarsened greatly. This microstructural evolution at 620–630 C is shown in Fig. 6.

Precipitate evolution in CW 316 irradiated in EBR-II also differed from that of the SA material. At the lower doses, there are no cavities, there is less precipitation, and no radiation induced phases in the CW 316 at 500–630 C (compare Tables 2 and 3). At 500–525 C, a few η phase particles are present after 8.4 dpa, while a dense mixture of small η and Laves precipitates develops at 620–630 C after the same dose. Occasional $M_{23}C_6(\tau)$ particles are also seen at the grain boundaries at 500–630 C. Precipitate evolution at 500–530 C is illustrated in Fig. 4b. A large amount of coarser η forms in the matrix with fine Laves laths after 36 dpa. The η-phase remains stable with increasing dose to 69 dpa, while more Laves develops as irregular or blocky particles attached to voids and radiation induced G and γ′ phases form. At 620–630 C, abundant coarser η and Laves

plus occasional large τ precipitate particles developed after 36 dpa, as shown in Fig. 6a through 6d. After 75 dpa, the precipitate microstructure has become very coarse (see Fig. 6e and 6f); most of the particles are η and Laves, but there are also some huge τ and σ phase particles.

Fine bubbles are observed throughout the matrix and along dislocations and precipitate/matrix interfaces, at 500–630 C after 36 dpa. However, they are absent among the well developed void structures found at higher fluence. No loops are observed in any of the CW specimens and the dislocation density exhibits little temperature dependence (see Table 3). The dislocation network recovers with dose between 8.4 and 36 dpa, and then remains constant at higher fluence.

Three important differences can be singled out relative to the microstructural evolution of SA material: 1) no loop microstructure develops, 2) void formation is delayed to higher dose; 3) the radiation induced phases G and γ′ evolve at high dose at 500–530 C while in SA material they have disappeared after 31 dpa. Development of the radiation induced phases in the CW 316 at 500–530 C comes during or after significant void evolution, suggesting a possible correlation between them.

Helium preinjected SA and CW (DO-heat) 316 — Helium generation rates in steels irradiated in current fast breeder reactors are much lower (~20–30 times) than those projected in the first wall of potential fusion reactors. The effects of increased helium generation on the microstructural evolution in steels, at reactor damage rates, have therefore been

investigated under the fusion materials program. The specimens were injected at room temperature by cyclotron irradiation with 60 MeV α-particles prior to the reactor irradiation. An energy degrader wheel was used to produce a uniform through-thickness distribution of helium. This preinjection results in a very high concentration ($>10^{23}$ m^{-3}) of fine (~2.2 nm in diam) interstitial Frank loops [8]. Helium preinjection of 110 and 200 at. ppm does not change the CW 316 microstructure [29], where a dense dislocation network is already present. Helium bubbles are not resolved in either type of as-injected material. Table 4 summarizes the microstructural evolution observed under EBR-II irradiation.

Helium preinjection suppresses void formation and causes a tremendous enhancement of fine bubble precipitation after 8.4 dpa at 500 and 625 C in SA 316, in comparison with uninjected material. Figure 7 illustrates these effects after irradiation at 625 C. Whereas at 500 C a dense Frank loop structure is seen, which appears to have evolved from the as-injected condition, at 625 C no loops are present; instead, a lesser dislocation network than in uninjected specimens has developed.

At 500 C, helium preinjected material exhibits no precipitates after 8.4 dpa. By contrast, at 625 C, more and coarser η and Laves phase particles form relative to uninjected material. Radiation induced phosphides do not form in the preinjected steel at 625 C.

Preinjected CW 316 does not exhibit any resolvable bubbles after 8.4 dpa at 500 C, similar to uninjected material, but a high concentration of fine bubbles does evolve after the same dose at 625 C. The dislocation evolution is, at both temperatures, about the same as in uninjected specimens, i.e., network recovery takes place. At 500 C, the sparse η-phase

precipitates found in uninjected CW 316 do not form, while a few coarse Laves particles are seen in the injected steel. However, at 625 C smaller η and Laves particles form more abundantly in the preinjected CW 316. Similar but coarser precipitates are observed at the same temperature and dose in preinjected SA 316.

HFIR Irradiations

In this water cooled and moderated reactor, high fluxes of both fast and thermal neutrons are found in irradiation positions directly adjacent to the fuel. Thermal neutrons produce helium via a two step nuclear reaction with ^{58}Ni at a rate of 10–70 appm/dpa, which is approximately two orders of magnitude higher than that generated during irradiation in EBR-II. The effects of helium in HFIR irradiated material can be determined by comparing with observations on the same material irradiated in EBR-II at similar temperatures and to the same fluence. Furthermore, a comparison with results on preinjected and EBR-II irradiated specimens permits the study of the influence of helium injection mode, e.g., helium buildup concurrent with displacement damage at the irradiation temperature vs cold injection prior to neutron irradiation. The thermal neutrons in HFIR also induce transmutation of some elements whereby the alloy chemistry slowly changes during irradiation. There is some vanadium production (0.61% at ~520 C and 61 dpa) and manganese burnout (1.33% remains at the same temperature and dose) [36], which do not occur in EBR-II.

SA (DO-heat) 316 – At doses below ~20 dpa, voids are found only at 425–450 C. After 9.2 dpa, most larger voids are attached to similarly

sized η-phase particles (Fig. 8a) but there are also many smaller matrix voids. After 14.3 dpa, the void and η-particle microstructures coarsen, as shown in Fig. 8b. Fine radiation induced γ′ particles are also present at this temperature together with Frank loops (Table 5). Both persist from 9.2 to 14.3 dpa, but neither is observed at higher temperatures.

From 515–555 C up to 625–650 C, the η and Laves particles are coarse over the dose range of 10 to 47 dpa, and yet voids are observed only after 47 dpa. In addition to large voids attached to η and Laves particles there are also 3 to 20 times more matrix voids which are 2 to 7 times smaller. Swelling is appreciable, as shown in Table 5 and Fig. 1.

At 615–640 C precipitation of τ-phase particles is also observed. At this temperature, the dislocation network is about ten times less dense than that at 450 C. At still higher temperatures (730–755 C) no voids are seen after 53 and 68.5 dpa, while precipitation of σ and τ-phase particles has taken place and the dislocation network has a very low density.

Fine bubbles are observed after irradiations at 425–640 C. Above 450 C they coarsen with increasing temperature and fluence, though bubble formation is sluggish at 615–640 C. At 730–755 C at high doses, swelling is due to coarse matrix bubbles and huge grain boundary bubbles.

Relative to EBR-II, we notice that after HFIR irradiation at 500–640 C neither irradiation induced phases (Fig. 4c), nor loops or voids are produced at the lower fluence. Many more bubbles nucleate early in HFIR but void formation is only enhanced at higher fluence.

20% CW (DO-heat) 316 — Voids develop after irradiation at temperatures below 500 C (Table 6 and Fig. 5). Matrix voids and a few bubbles are found after 8.4 dpa at 325–350 C, whereas at 425–450 C and 9.2 dpa matrix voids occur together with many fine matrix bubbles (Fig. 8c). After 14.3 dpa at 425–450 C, however, only fine matrix bubbles are observed (Fig. 8d). But matrix voids and large voids associated with η-phase precipitates are seen again together after 55 dpa. At 500–640 C a fine dispersion of subcritical bubbles, that remains stable with increasing fluence (up to 47 and 61 dpa), is observed throughout the matrix. Above 650 C, the CW specimens recrystallize under irradiation and their microstructure evolves similarly to that of the initially SA material described in the preceding subsection.

No precipitation is observed after 8.4 dpa at 325–350 C (Table 6). Fine radiation induced γ' particles are seen, together with matrix voids, only after 9.2 dpa at 425–455 C. This phase is not observed either at higher fluences (see Fig. 8) or at higher temperatures. At higher fluences, stable η-phase particles are present from 14.3 to 55 dpa. At higher temperatures (500–650 C) abundant mixtures of coarse η, τ, and Laves phase particles, with compositions similar to those obtained during thermal aging, rapidly form and persist to high fluences (Fig. 4d).

Frank loops are found together with voids after 8.4 dpa at 325 C. They are also seen after 9.2 dpa at 450 C together with matrix voids, bubbles and the γ' particles. Frank loops are not observed either at higher fluences or higher temperatures. Over the temperature range

425–650 C, the dislocation network recovers with fluence to a concentration of 0.8–2 × 10^{14} m/m^3.

Void development in CW specimens is delayed relative to SA 316 irradiated in HFIR at 425–640 C (Fig. 9a and 9b) and to CW samples irradiated in EBR-II at 500–640 C (Fig. 9b and 9c). Although many more helium bubbles nucleate much earlier in HFIR, they apparently remain below the critical size for void conversion up to 47–61 dpa. Precipitation also develops differently in HFIR and in EBR-II. Laves formation is enhanced in HFIR at 500–550 C, while σ is enhanced at 600–640 C. HFIR irradiation also produces fine τ precipitation, which is not found after EBR-II irradiation either in uninjected or in helium preinjected specimens.

20% CW (N-lot) 316 — The microstructural evolution of HFIR irradiated 20% CW (N-lot) 316 steel is quite different from that of HFIR irradiated 20% CW (DO heat) 316 (Table 7 and Fig. 5). At 300 C, no bubbles or voids are seen after 10 dpa. High concentrations of very fine bubbles are found above 400 C at all fluences (at 300 C, after 44 dpa). Bubbles coarsen with fluence at 600 C but remain stable at 400 and 500 C. Matrix voids begin to form after ~22 dpa at 400 C and after ~10 dpa at 500 and 600 C. At higher fluences (44 dpa at 400 and 500 C and 22–44 dpa at 600 C) very coarse voids develop on large η-phase particles that formed along intragranular faulted bands.

No precipitation is observed at 300 C up to a fluence of 44 dpa. At 400 C, no precipitates are detected after 10 dpa. Some fine MC (possibly

VC) particles develop after 22 dpa, while fine γ' and coarser η (along faulted bands) are found after 44 dpa. At 500 and 600 C, fine γ' precipitates are observed at 10–22 dpa, but they have dissolved after 44 dpa. By contrast, η-phase particles form (in the matrix) after 22 dpa at 500 C and 10 dpa at 600 C and increase their volume fraction and size with fluence at both temperatures.

Frank loops are observed after all irradiation doses at the four temperatures, except at 600 C after 44 dpa. The dislocation loop and network concentrations decrease significantly with increasing fluence only at 600 C.

Void formation in the N-lot CW steel is enhanced and shifted to higher temperatures relative to the CW DO-heat material during HFIR irradiation. Irradiated N-lot specimens not only exhibit a finer matrix bubble distribution but also have many more loops and show dislocation network recovery at 600 C. The precipitation of the radiation induced γ'-phase is enhanced relative to the DO-heat steel. Moreover, the CW (N-lot) 316 does not develop either Laves or τ-phase precipitates during HFIR irradiation; the absence of Laves is consistent with thermal aging studies of this steel which reveal that it is much less prone to Laves formation than the DO-heat steel [37].

GENERAL SURVEY OF COMPOSITIONS OF PRECIPITATE PHASES

A complete characterization of precipitate nature and evolution under irradiation involves phase identification, compositional determination and

related microstructural development. Here, we emphasize phase identity and composition, as these may reveal the underlying processes involved in forming the phase under irradiation.

Precipitation under thermal aging is briefly presented in order to evaluate the changes that occur under irradiation. The nature and composition of the phases are described within a phenomenological classification [8,12,23]. In the type 316 stainless steels, τ, σ, and χ are usually radiation-retarded, η and Laves are radiation-enhanced in some cases and modified in others, while γ', G and the phosphides are radiation-induced [8,23]. The compositional differences relative to those under thermal aging suggest the occurrence of a segregation process characteristic of an irradiation environment. Radiation induced segregation (RIS) is a nonequilibrium transport of solute atoms due to their interaction with the radiation induced point defects and their sinks. RIS produces Ni and Si enrichment and Mo and Cr depletions, and these effects can be recognized particularly in the compositionally modified phases.

Thermal Aging

Various phases precipitate in SA and CW (DO-heat) 316 after aging at 550–900 C for several thousand hours. The precipitate microstructure coarsens with increasing temperature [8]. In SA material, $M_{23}C_6$ (τ) dominates

at 560– 600 C and Laves particles dominate at 650–700 C; χ and σ are the most abundant at higher temperatures. Small amounts of M_6C (η) and σ also occur together with τ and Laves after 10,000 h at 650 C. Cold working generally enhances the formation of Laves, η and σ phases, while refining the precipitate microstructure [8,29]. In 20% CW 316, τ again dominates at 560 C, but Laves is predominant at 600–700 C, with increasing amounts of η and σ relative to SA 316.

The compositions of the thermal phases τ, η, σ, Laves, and χ are rich in either molybdenum or chromium or both and depleted in nickel (except for η) and iron relative to the matrix. Laves and η are rich in silicon, while τ is usually poor in it. Compositions of several of the phases formed in SA and CW (DO-heat) 316, aged for 2770–4400 h and analyzed on extraction replicas by AEM, are given in Tables 8 and 9.

On a relative basis, τ has the highest chromium, η the highest silicon and nickel, while Laves has the most molybdenum and σ and χ contain the most iron. The broad beam analyses in Table 8 are compositional averages of many precipitate particles that provide information on their relative abundance [8,38]. During aging, although the precipitate microstructure changes with temperature, time, and initial metallurgical condition, the phase compositions experience little change in the range 500–700 C.

The precipitation patterns of SA (DO heat) 316 and SA (N-lot) 316, after 166 h aging at 800 C, were found to be somewhat different (see Table 1 for heat compositions). The DO-heat specimens exhibited coarse matrix τ, Laves, and χ particles together with τ at the grain boundaries,

whereas the N-lot samples only precipitated τ-phase particles at the grain boundary [37]. The DO-heat appears to be more unstable toward precipitation and more prone toward intermetallic phases than the N-lot. Previous studies comparing the DO-heat with other 316 heats also reached similar conclusions [8].

EBR-II Irradiation

Irradiation of SA material at 500 C induces γ', G and a phosphide phase (A-type) after 8.4 dpa, but only the phosphide needles persist to 31 dpa (Table 2). Both G and γ' have very high nickel and silicon contents and are depleted in chromium relative to the matrix; G has more molybdenum and manganese than γ'. There appear to be two phosphides, distinguished primarily on the basis of compositional differences, A and B as seen in Table 9 [8]. The A-phosphide also has high silicon and nickel contents. At 625 C, the radiation induced B-phosphide develops after 8.4 dpa but does not survive at higher fluence. The B-phosphide contains much less silicon and nickel than the A-phosphide, but more molybdenum, chromium, and iron.

At 500 C, η is the most abundant phase and is modified. It has significantly less molybdenum than the thermal phase. Its volume fraction increases with fluence. At 625 C, η formation is enhanced and persists to higher fluence as Laves develops. Laves is also modified, having more nickel and less molybdenum than the thermal Laves. Under all the irradiation conditions studied here, SA material did not precipitate the

τ-phase in the matrix. Phase evolution and compositions suggest that RIS effects are most significant at lower temperatures and fluence.

In CW-316, the radiation induced γ′ and G phases are seen at 500–525 C after 69 dpa, but not after the lower fluences. These phases have similar compositions to those appearing in the SA samples. Laves and η also develops at this temperature. Laves becomes highly modified as fluence increases (lower chromium, iron and molybdenum, more silicon and nickel). At ~625 C, η and Laves develop and coarsen considerably with fluence from 8.4–75 dpa (see Fig. 6). Both phase compositions are nearly thermal from 8.4 to 36 dpa but Laves becomes strongly modified at 75 dpa. Again, τ precipitation is retarded relative to aged CW 316 material. Precipitation in CW 316 suggests that there is a strong influence of the early dislocation microstructure which affects the development of RIS.

Helium preinjection eliminates virtually all precipitation at 8.4 dpa and 500 C in both SA and CW 316, but enhances η and Laves formation at 625 C. Such enhanced precipitation can be seen in Fig. 7 together with the tremendous increase in bubble nucleation. In this case, RIS appears to be suppressed.

HFIR Irradiation

Radiation-induced γ′ is observed at 425–450 C during HFIR irradiation of SA 316, after 9.2 and 14.3 dpa. At 425–550 C, the formation of η is enhanced, whereas Laves is enhanced at 525–550 C. Thermal precipitation of η, Laves and τ occurs during irradiation at 600–640 C. The compositional modification of η is sensitive to irradiation temperature as

molybdenum content increases with increasing temperature, but not to fluence. The Laves phase composition is sensitive to both temperature and fluence; it becomes more modified (higher nickel and silicon, less molybdenum) with fluence at 515–555 C, but is present with the thermal composition at 600–640 C. Relative to EBR-II irradiation at 500–640 C, the precipitation phenomena in HFIR show less effects of RIS and more "thermal" behavior at lower doses at 500–550 C.

In 20% CW 316, the presence of γ' is transient while modified η forms more sluggishly at 425–450 C than in the SA material. At 500 C and above, the precipitate microstructure consists of a mixture of enhanced thermal phases, viz. Laves, η and τ, whose compositions remain unchanged as fluence increases from 47 to 61 dpa (Table 9). At 500–550 C, τ formation is enhanced, in contrast to its retardation in HFIR irradiated SA specimens and EBR-II irradiated SA and CW samples. Figure 6 illustrates the abundance of Laves formation in the 20% CW 316 in HFIR at 500–550 C, while Fig. 10 highlights its stationary composition with increasing fluence, in contrast to its evolution with fluence in EBR-II (compare Tables 3, 4, and 6). HFIR irradiation enhances thermal precipitation in CW 316 at 500–640 C, with little evidence of RIS.

ANALYSIS OF EXPERIMENTAL RESULTS

Although the ensemble of experimental results is fairly complex in its details, there appear to exist some general interrelationships among the

various microstructural evolutions that take place under irradiation. Voids are always larger when they are attached to precipitate particles. However, coprecipitation of void and particle is one of several possibilities. Coprecipitation seems to be the case in SA (DO heat) 316 irradiated in EBR-II at 500 C, where the number of equally sized void and η particle pairs increases with fluence. But the precipitate particles can develop first, e.g., η and Laves form before voids become attached in SA (DO heat) 316 irradiated in HFIR at 500–550 C. Or, voids may develop first, as seems to be the case in 20% CW (DO heat) 316 irradiated in EBR-II at 510 to 69 dpa, where G and Laves particles are seen in association with voids.

The experimental observations appear to indicate that the formation of precipitate associated voids correlates with the evolution of the other components of the microstructure. At low fluences, voids develop in conjunction with Frank loops and radiation-induced phases in SA material and in 20% CW (N-lot) 316. However, in the presence of other microstructural features, voids are not observed to develop. An inspection of Tables 2–6 shows that either too many bubbles or too many dislocations are found instead of voids. But in 20% CW (N-lot) 316 irradiated in HFIR, the codevelopment of γ′ and many loops again coincides with abundant void formation despite the presence of many fine bubbles. Fine bubble nucleation alone is thus not sufficient to suppress void formation. It is also necessary that they be prevented to reach the critical radius for bias driven growth. The observed coupling of voids, radiation induced precipitates and loops

diminishes as voids form without these other phenomena at higher irradiation temperatures and fluence. At higher fluences during HFIR irradiation, with the exception of 20% CW (DO heat) 316, bubbles coarsen or dislocation structures eventually recover and voids then develop in the matrix as well as attached to precipitate particles.

A second important aspect relevant to precipitate void associated development is the nature and stability of the phases that precipitate in the irradiation environment. The present data, as well as previous study [8], suggest that RIS can be the strongest influence on phase formation and composition in neutron irradiated steels that contain voids. The radiation-enhanced modified or induced phases do not uniquely correlate with positive or negative misfit [Table 9]. Enhanced thermal diffusion effects are manifest only when RIS is suppressed. The data further show, in the heats of steel examined, that voids form only in association with radiation induced G or phosphide phases, radiation modified Laves and radiation enhanced or modified η-phase. This therefore makes clear the connection between RIS and precipitate-void association. On the other hand, the fact that γ' does not exhibit PVA indicates that there are other factors to consider than simply being a radiation-induced phase for the phenomenon to occur.

The nature of the phases associated with voids makes their formation and stability at least sensitive to irradiation conditions that affect RIS. In many cases η-phase particles form and remain stable with fluence and voids eventually associate with them in both EBR-II and in HFIR, unless

helium induces what appears to be a bubble dominated sink structure. Laves phase particles at 500–550 C in EBR-II or HFIR are associated with voids when they are highly radiation modified. Enhanced Laves particles are coarse and abundant at 500–550 C in CW (DO heat) 316, and yet have no voids or compositional modification. Both facts can be connected to the development of many matrix bubbles that dominate the sink structure. This establishes a very large critical radius, increases the critical number of gas atoms for bubble to void conversion and retards the accumulation of that number in the cavities. Moreover, the formation of τ, in particular, appears to be a significant indication that RIS processes are not operative, consistent with enhanced thermal processes and no precipitate-associate voids.

DISCUSSION

It was concluded from our analysis of experimental results that the evolution of the total microstructure occurs in a correlated and interactive manner. The observations define a fairly complex phenomena space for PVA under the various specific constraints. The reasonable common factor, however, affecting all the aspects of microstructural evolution under irradiation is the point defect behavior. Mechanisms involving point defects can therefore be suggested that explain precipitate-void association and its relationship to other aspects of microstructural development.

Theoretically and experimentally it is well established that there are different paths for decreasing the number of radiation induced point defects besides vacancy-interstitial recombination. Some of these paths can lead to the formation of various microstructural features which in turn also operate as point defect sinks. The formation of dislocation loops and of voids, for instance, indicate the aggregation of like-point defects which escape Frenkel pair recombination. Another path for point defect annihilation is by absorption at sinks, e.g., grain boundaries and dislocations. But in this case, imbalanced interstitial vs vacancy absorption at the sinks affects their evolution, as for example, the deformation produced dislocation microstructure of initially CW material recovers during irradiation.

A key point of radiation induced microstructural evolution is imbalanced absorption of vacancies and interstitial at sinks, as demonstrated by the cooperative development of various microstructural components. Independent of the difference in vacancy and interstitial diffusivities, the quasi-steady state fluxes of both types of point defects to sinks are the same unless some sinks are biased for one type of point defect. This is a well established result from rate theory as applied to void swelling [11].

Analogous to void formation we propose that radiation-induced precipitation can be explained by the presence of sinks which have different biases for different interstitial species. Dislocations are biased for interstitials relative to vacancies. The origin of the bias is the elastic

interaction between the interstitial and the dislocation. In a multicomponent system, larger self-interstitial atoms produce a larger strain field than smaller ones. Hence, it can be suggested that dislocations will exhibit a greater bias for larger interstitial species than for smaller ones. This means that the capture radius of dislocations for larger interstitials is greater than for smaller ones. This differential bias may then give rise to an inhomogeneity in the spatial content of different interstitial solute species that constitutes the RIS phenomenon.

From our results the formation of Frank loops is, in most cases, correlated with development of voids, γ' and/or G-phase precipitation. The formation of loops during early irradiation of SA material establishes a biased sink in the system. Since nickel and silicon are undersized solutes, the following effects can be envisaged. The greater capture radius of larger self-interstitials by loops leads to a higher probability of forming clusters of smaller self-interstitials elsewhere in the matrix. Also, an atmosphere of smaller solutes could build up reducing the lattice dilation around the loop hence lowering its strain energy [39]. In the case of the DO-heat and the N-lot, the formation of clusters leading to precipitates appears to be favored away from loops.

The presence of the biased sinks enhances cluster evolution. Moreover, clusters enriched with smaller solutes can grow to larger sizes than those enriched with larger solutes. Since self-interstitial clusters produce a compressive strain field, they may also attract vacancies to relieve the strain. At a given size, the cluster should become unstable and precipitate into a nickel and silicon rich phase.

The clustering process just described can most easily produce phases that are crystallographically related to the γ-matrix and coherent with it. This is indeed the case of γ′. Although the nucleation process of the radiation induced phosphides is similar, these phases have a different crystalline structure than the matrix and much less nickel than γ′ and G, as shown in Table 9.

Under EBR-II irradiation, coherent γ′ and randomly oriented G are observed at the same fluences indicating that clusters that will precipitate into them are forming at the same time. These two phases do, however, differ in their PVA behavior. As can be seen in Tables 8 and 9, their composition is fairly similar, except for molybdenum and manganese, which are higher in G, and silicon which is higher in γ′. Similarly, the compositions of the phosphides show a higher molybdenum content than γ′. This difference in composition may explain why voids are attached to G and the phosphides but not to γ′.

During the clustering stage, the presence of more oversized atoms, such as molybdenum, may attract more vacancies than a neutral sink and this effect is further enhanced because there is a vacancy excess sustained in the matrix by the biased sinks. The presence of a vacancy cloud at the cluster can, in turn, be stabilized by gaseous impurities. In this unique cooperative process, a solute rich cluster and a void embryo may codevelop and give rise to precipitate void association.

Continued precipitation and/or growth of these radiation induced phases depends critically on the RIS level that is maintained in the

matrix. If microstructural evolution alters the level of RIS, it may also affect the stability of those phases. Thus, when loops start unfaulting and other loops no longer form, the intense RIS that resulted from loop formation is no longer sustained. Instability of the radiation induced phases γ' and G is then a logical outcome because their environment has changed dramatically. "Thermal" mechanisms, which tend to restore equilibrium, operate to a larger degree leading to dissolution of the induced phases.

The nucleation of the other radiation modified or enhanced phases (η and Laves) can be explained by a similar mechanism as that employed for the G phase. While both exhibit PVA behavior, their own stability is not as sensitive to changes in the evolution of the surrounding microstructure. This characteristic suggests that these phases are the result of RIS in conjunction with thermal mechanisms such as normal solute diffusion that are enhanced by irradiation. The influence of RIS is nicely exemplified by Laves phase evolution in SA 316 during HFIR irradiation at 515–555 C. In this case, the modification of the phase at higher doses and the evolution of attached voids under this condition is an indication of a delayed RIS process.

The early precipitation of η, whether modified or not, is apparently related to the inhibition of the τ-phase, since the latter appears to be incompatible with RIS. Tau precipitation is delayed because the clusters that are favored under irradiation are those incorporating nickel and silicon. Eta-phase precipitation constitutes, in the irradiation environment,

a similar lattice response from the viewpoint of crystal structure as that of τ formation. In fact, in early phase identification studies, η-phase particles were classed as modified, nickel-rich, τ precipitates (see discussions in Ref. [8]). The crystallographic difference between the two was later revealed by noting the missing (200) reflections in the η (011) zone axis pattern.

Helium effects, although fairly complex, reinforce several aspects of the suggested mechanism of precipitate-void association. During HFIR irradiation of DO-heat 316 steel, loop evolution and γ' precipitation are observed only at the lower temperatures, e.g. ~420 C. At higher temperatures, an abundant bubble population delays conversion of the bubbles to voids in both SA and CW material. In fact, at 61 dpa voids are still not observed in the CW (DO-heat) 316 (see Table 6). These effects seem due to a high sink strength of the bubbles which then enhances point defect recombination and partitions helium to more bubbles. Such recombination at many sites would also dilute RIS, preventing the formation of radiation induced phases and further frustrating the conversion of bubbles to voids [12].

Observations in the HFIR irradiated N-lot specimens further emphasize the competition of sinks for point defect absorption. In contrast to the observed microstructural evolution of the DO steel, the cold worked N-lot samples do not exhibit much dislocation network recovery. This could result from the poisoning of climbing sites at dislocations suggested by compositional differences between alloys. Such an effect tends to cancel the bias and limit point defect absorption at dislocation sinks. Or, it

could be that the difference in alloy compositions affects loop formation itself. In either case, increased loop formation could favor increased RIS evolution, which in turn promotes γ' formation. Such conditions restore the bias and allow bubble conversion into voids both in the matrix and in association with precipitates.

The phenomenon of PVA was only observed on G, η, Laves and phosphide particles in the irradiated steels described here. We may question whether or not the phase crystallography, the volume misfit, the nature of the particle/matrix interface or the phase composition determine void association with the particle. Although for a given steel composition, these aspects are all interrelated, some of these effects appear more important than others. Volume misfit has not been determined precisely for the precipitates formed under irradiation, but is inferred from either the thermal phase or the ideal compound. Both positive (e.g. G and η) and negative (Laves and M_2P) phases are associated with voids. On the other hand, γ' and τ with negative and positive misfits, respectively, are not. So volume misfit does not seem to be a determining factor.

The overall nature of the particle/matrix interface cannot be separated from the chemical composition and the nature of the phase itself. In particular, in the model we have proposed, the diffusion of certain solutes to the particle, which controls its growth, also brings a vacancy surplus. Codevelopment of precipitate and void must be compatible with the interface nature. If the phase does not remain stable, codevelopment is disrupted and the void becomes a matrix void. Phase nature and

compositions do at least appear crucial to associated development of phase particles and voids. Subtle compositional differences for a given phase may also result in different behavior in other alloys. For example, voids do associate with γ' particles during neutron irradiation of another heat of type 316 austenitic stainless steel, with a higher titanium content than DO and N steels, as shown in Fig. 12 [40].

CONCLUSIONS

Precipitate-void association has been studied in a large number of experiments done with a single heat (DO) type 316 austenitic stainless steel. Here, we have analyzed the experimental results with a focus on PVA and its relation to the evolution of other microstructural components. We have concluded that PVA is strongly related to the overall microstructural evolution. It may therefore be stated that not only the point defect generation characteristics determine the microstructure or alter precipitate behavior under irradiation, but also the kinetic features of point defect annihilation.

The nucleation and growth of radiation induced, modified and enhanced phases exhibiting high nickel and silicon contents and low molybdenum and/or chromium lead us to suggest a precipitation mechanisms that can also describe precipitate-void codevelopment. We proposed that there exists not only a biased attraction of interstitials by dislocations relative to vacancies but also a differential bias among self-interstitials caused by the size differences among the various atomic species. Similar to the case

of void formation, such a mechanism would allow the formation of clusters rich in undersized solute species that then lead to precipitation. PVA can arise when a surplus of vacancies and possibly gas impurities add to the cluster in order to relieve its strains.

Phase composition and the related nature of the precipitate/matrix interface appear from the data to play a vital role in PVA. Furthermore, the different microstructural evolution under HFIR irradiation in DO and N steels demonstrates the importance of chemical composition of the bulk alloy, particularly as it influences dislocation evolution. Such differences support the competitive nature of various components whose balance determines microstructural development during irradiation.

ACKNOWLEDGEMENTS

We would like to thank Dr. T. C. Reuther for supporting the reactor experiments over ~10 years through the Alloy Development Program of the Office of Fusion Energy, U.S.D.O.E. We also thank N. B. Rouse for specimen preparation at ORNL. We are grateful to Drs. E. H. Lee, R. E. Stoller, L. K. Mansur, and W. Kesternich (on assignment from KFA-Jülich) at ORNL and Professor A. J. Pedraza at the University of Tennessee for helpful reviews and discussions.

REFERENCES

1. C. Cawthorne and E. J. Fulton, "The Influence of Irradiation Temperature on the Defect Structures in Stainless Steel," pp. 446–460 in Symp. The Nature of Small Defect Clusters, Vol. 2, ed., M. J. Makin, AERE Harwell, AERE-R-5269 (1966).

2. L. K. Mansur, M. R. Hayns, and E. H. Lee, "Mechanisms Affecting Swelling in Alloys with Precipitates," pp. 359–382 in Conf. Proc. Phase Stability under Irradiation, eds., J. R. Holland, L. K. Mansur, and D. I. Potter, The Metallurgical Society of AIME, Warrendale, PA (1981).

3. L. K. Mansur, Phil. Mag. A44 (1981) 867–877.

4. G. R. Odette, P. J. Maziasz, J. A. Spitznagel, J. Nucl. Mater., 103&104 (1981) 1289–1304.

5. A. F. Rowcliffe and E. H. Lee, J. Nucl. Mater. 108&109 (1982) 306–318.

6. R. E. Stoller and G. R. Odette, "The Effect of Helium on Swelling in Stainless Steel: Influence of Cavity Density and Morphology," pp. 275–294 in Effects of Radiation on Materials: Eleventh Conference, eds., H. R. Brager and J. S. Perrin, American Society for Testing and Materials, ASTM-STP-782 (1982).

7. G. R. Odette and R. E. Stoller, J. Nucl. Mater., 122&123 (1984) 514–519.

8. P. J. Maziasz, "Effects of Helium Content on Microstructural Development in Type 316 Stainless Steel Under Neutron Irradiation," Oak Ridge National Laboratory Report, ORNL-6121, Nov. 1985.

9. H. R. Brager and J. L. Straalsund, J. Nucl. Mater. 46 (1973) 134–158.

10. E. E. Bloom and J. O. Stiegler, "Effect of Irradiation on the Microstructure and Creep-Rupture Properties of Type 316 Stainless Steel," pp. 360–382 in Effects of Radiation on Substructure and Mechanical Properties of Metals and Alloys, ASTM-STP-529, American Society for Testing and Materials (1973).

11. A. D. Brailsford and R. Bullough, J. Nucl. Mater. 44 (1972) 121–135.

12. P. J. Maziasz, J. Nucl. Mater. 108&109 (1982) 359–384.

13. P. J. Maziasz, J. Nucl. Mater. 122&123 (1984) 472–486.

14. D. R. Arkell and P.C.L. Pfeil, J. Nucl. Mater. 12 (1964) 145–152.

15. J. A. Brinkman and H. Wiedersich, "Mechanisms of Radiation Damage in Reactor Materials," pp. 3–39 in Symp. Flow and Fracture of Metals and Alloys in Nuclear Environments, ASTM-STP-380, American Society for Testing and Materials, 1965.

16. R. S. Nelson, J. A. Hudson, and D. J. Mazey, J. Nucl. Mater. 44 (1972) 318–330.

17. P. R. Okamoto, S. D. Harkness, and J. J. Laidler, Trans. Am. Nucl. Soc. 16 (1973) 70.

18. C. Cawthorne and C. Brown, J. Nucl. Mater. 66 (1977) 201–202.

19. H. R. Brager and F. A. Garner, J. Nucl. Mater. 73 (1978) 9–19.

20. L. E. Thomas, Trans. Am. Nucl. Soc. 28 (1978) 151.

21. P. J. Maziasz, Scripta Met. 13 (1979) 621–626.

22. T. M. Williams and J. M. Titchmarsh, J. Nucl. Mater. 87 (1979) 398–400.

23. E. H. Lee, P. J. Maziasz, and A. F. Rowcliffe, "The Structure and Composition of Phases Occurring in Austenitic Stainless Steels in Thermal and Irradiation Environments," pp. 191–218 in Conf. Proc. Phase Stability During Irradiation, eds., J. R. Holland, L. K. Mansur, and D. I. Potter, The Metallurgical Society of AIME, Warrendale, PA (1981).

24. W.J.S. Yang, H. R. Brager, and F. A. Garner, "Radiation-Induced Phase Development in AISI 316," pp. 257–270 in Conf. Proc. Phase Stability During Irradiation, eds., J. R. Holland, L. K. Mansur, and D. I. Potter, The Metallurgical Society of AIME, Warrendale, PA, 1981.

25. T. M. Williams and J. M. Titchmarsh, J. Nucl. Mater. 98 (1981) 223–226.

26. T. M. Williams and P. W. Lake, "Some Characteristics of a Diamond Cubic Phase Commonly Observed in Irradiated Austenitic Steels," to be published in Conf. Proc. Dimensional Stability and Mechanical Behavior of Irradiated Metals and Alloys, 2, BNES, held April 11–13, 1983, London, England.

27. P. J. Maziasz, J. Nucl. Mater. 122&123 (1984) 236–241.

28. P. J. Maziasz and D. N. Braski, J. Nucl. Mater. 122&123 (1984) 311–316.

29. P. J. Maziasz, J. A. Horak, and B. L. Cox, "The Influence of Both Helium and Neutron Irradiation on Precipitation in 20%-Cold-Worked Austenitic Stainless Steel," pp. 271–292 in Conf. Proc. Phase Stability During Irradiation, eds., J. R. Holland, L. K. Mansur, and D. I. Potter, The Metallurgical Society of AIME, Warrendale, PA, 1981.

30. P. J. Maziasz, "Microstructural Development in 20%-Cold-Worked Types 316 and 316 + Ti Stainless Steels Irradiated in HFIR: Temperature and Fluence Dependence on the Dislocation Component," pp. 54–97 in ADIP Quart. Prog. Rept., Sept. 30, 1981, DOE/ER-0045/7, Office of Fusion Energy, U.S. DOE.

31. P. J. Barton, B. L. Eyre, and D. A. Stow, J. Nucl. Mater. 67 (1977) 181–199.

32. T. A. Kenfield, W. K. Appleby, H. J. Busboom, and W. L. Bell, J. Nucl. Mater. 75 (1978) 85–97.

33. E. H. Lee, A. F. Rowcliffe and E. A. Kenik, J. Nucl. Mater. 83 (1979) 79–89.

34. J. I. Bramman, et al., "Void Swelling and Microstructural Changes in Fuel Pin Cladding and Unstressed Specimens Irradiated in DFR", pp. 479–507 in Radiation Effects in Breeder Rector Structural Materials, eds., M. L. Bleiberg and J. W. Bennett, TMS-AIME, New York (1977).

35. L. LeNaour, M. Vouillon, and V. Levy, "Influence of Dose and Dose Rate on the Microstructure of Solution-Annealed 316 Irradiated Around 600°C," pp. 310–324 in Effects of Irradiation on Materials: Eleventh Conf., ASTM-STP-782, American Society for Testing and Materials, 1982.

36. H. R. Brager and F. A. Garner, J. Nucl. Mater. 108&109 (1982) 347–358.

37. P. J. Maziasz and S. Jitsukawa, "Minor Compositional Variations of the Austenitic PCA to Explore MC Formation and Stability Characteristics for Improved Radiation Resistance," pp. 37–48, ADIP Semiannual Prog. Rept., March 31, 1985, DOE/ER-0045/14, Office of Fusion Energy, U.S. DOE.

38. P. J. Maziasz and G. R. Odette, "Wide Area Beam Averaged AEM of Precipitate Particles Extracted on Replicas from Type 316 Stainless Steel," pp. 198–199 in Proc. Forty-First Annual EMSA Meeting, ed., G. W. Bailey, San Francisco Press, Inc., San Francisco, CA (1983).

39. E. A. Kenik, Scripta Met. 10 (1976) 733–738.

40. E. H. Lee, unpublished work, ORNL (1985).

FIGURE CAPTIONS

Fig. 1. Cavity swelling in reactor irradiated SA (DO heat) 316 stainless steel as a function of irradiation temperature and dose.

Fig. 2. Void and precipitate microstructure in EBR-II irradiated SA (DO-heat) 316 stainless steel, showing highest level of PVA (a) 31 dpa at 525 C and (b) 36 dpa at 630 C.

Fig. 3. Examples of precipitate-void association: (a) η-phase, (b) G-phase, (c) Laves, and (d) phosphides.

Fig. 4. Precipitate volume fractions in reactor irradiated (DO heat) 316 stainless steel.

Fig. 5. Cavity swelling in reactor-irradiated 20% CW (DO heat and N-lot) 316 stainless steels as a function of irradiation temperature and dose.

Fig. 6. Void and precipitate microstructure of EBR-II irradiated 20% CW (DO-heat) 316 stainless steel at 620–630 C. (a) and (b): 8.4 dpa (no voids), (c) and (d): 36 dpa (η and Laves particles), (e) and (f): 75 dpa (η and Laves particles); (a), (c) and (e) are thin foil micrographs; (b), (d) and (f) are from extraction replicas. Notice codevelopment of the microstructure. Largest particles in (f) are τ and σ.

Fig. 7. Effects of 110 at. ppm helium preinjection on the microstructural evolution of EBR-II irradiated SA (DO-heat) 316 stainless steels to 8.4 dpa. at 625 C. (a) uninjected, low magnification, showing voids and precipitates, (b) preinjected, low magnification, showing no voids, (c) uninjected, high magnification, showing small bubbles at dislocations, (d) preinjected, high magnification, showing numerous bubbles at dislocations and throughout the matrix.

Fig. 8. Voids and η-phase particle microstructure in HFIR irradiated (DO-heat) 316 stainless steel at 450 C. (a) SA, 9.2 dpa, (b) SA, 14.3 dpa, (c) CW, 9.2 dpa, and (d) CW, 14.3 dpa. Voids and precipitates codevelop in the SA material. In the CW samples, they appear to have a transient character, as they both disappear at the intermediate dose of 14.3 dpa, showing the correlation in their evolution.

Fig. 9. Effects of helium and/or initial metallurgical condition on void development in irradiated (DO-heat) 316 stainless steel, at 500–550 C. (a) HFIR irradiation of SA material to 47 dpa, showing well developed voids and precipitates. (b) HFIR irradiation of CW material to 61 dpa, showing very abundant bubble and precipitate populations, but no voids. (c) EBR-II irradiation of CW material to 69 dpa, showing many voids and precipitates.

Fig. 10. Composition evolution of Laves phase in irradiated 20% CW (DO-heat) 316 stainless steel.

Fig. 11. Different microstructural patterns in two heats of 20% CW 316 stainless steel irradiated in HFIR at 600–625 C and 44–47 dpa. (a) DO-heat — abundant precipitation and bubbles. (b) N-lot — well developed voids.

Fig. 12. Advanced stage of cavity growth on γ′ particles in EBR-II irradiated SA (V7) 316 Ti-modified stainless steel (courtesy of Dr. E. H. Lee, ORNL).

ORNL-DWG 85-17867R

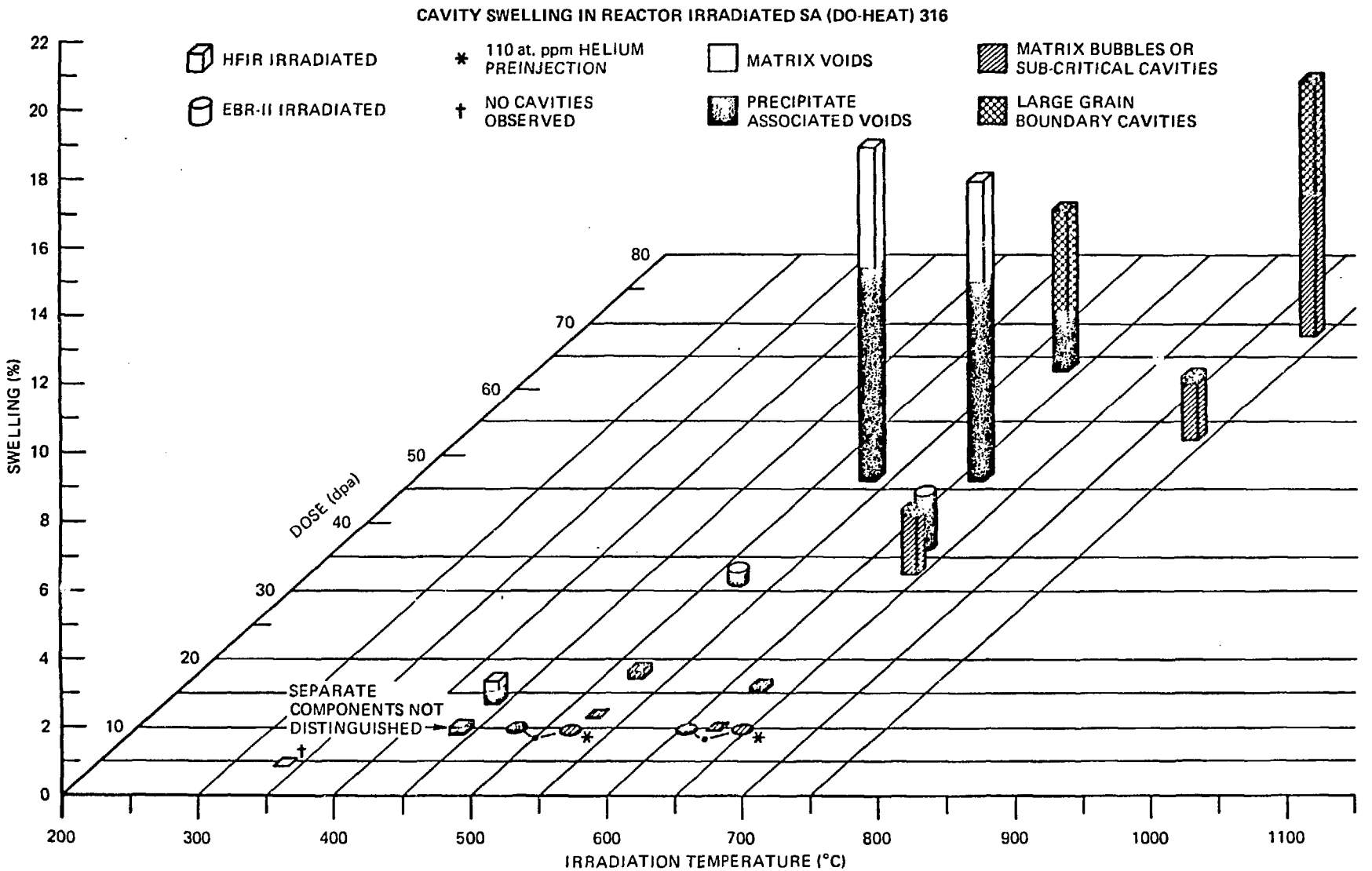

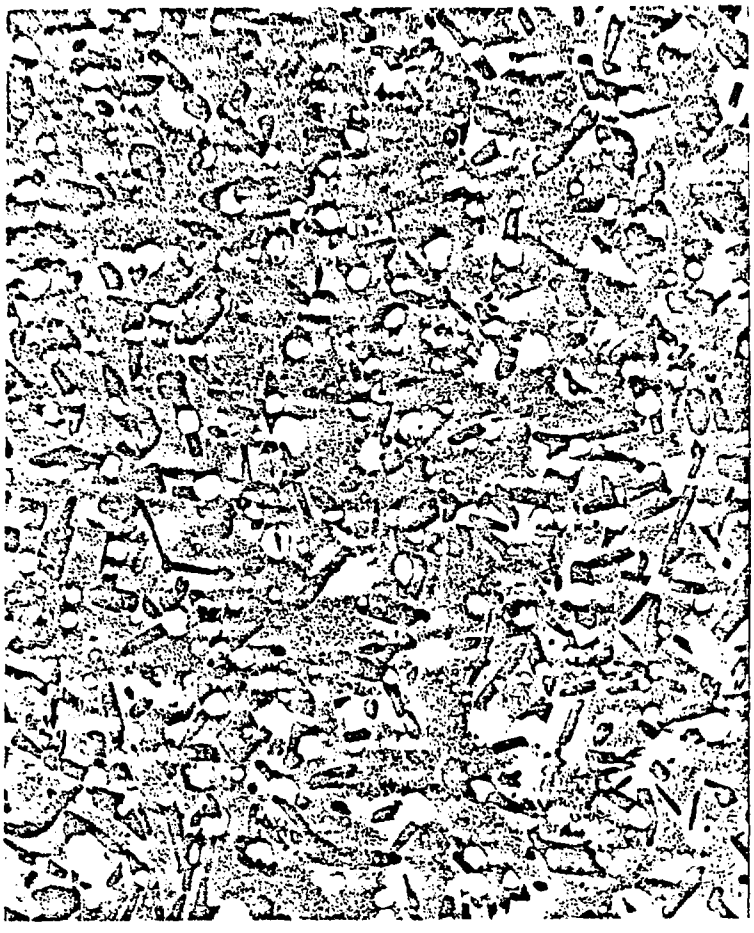

(b)

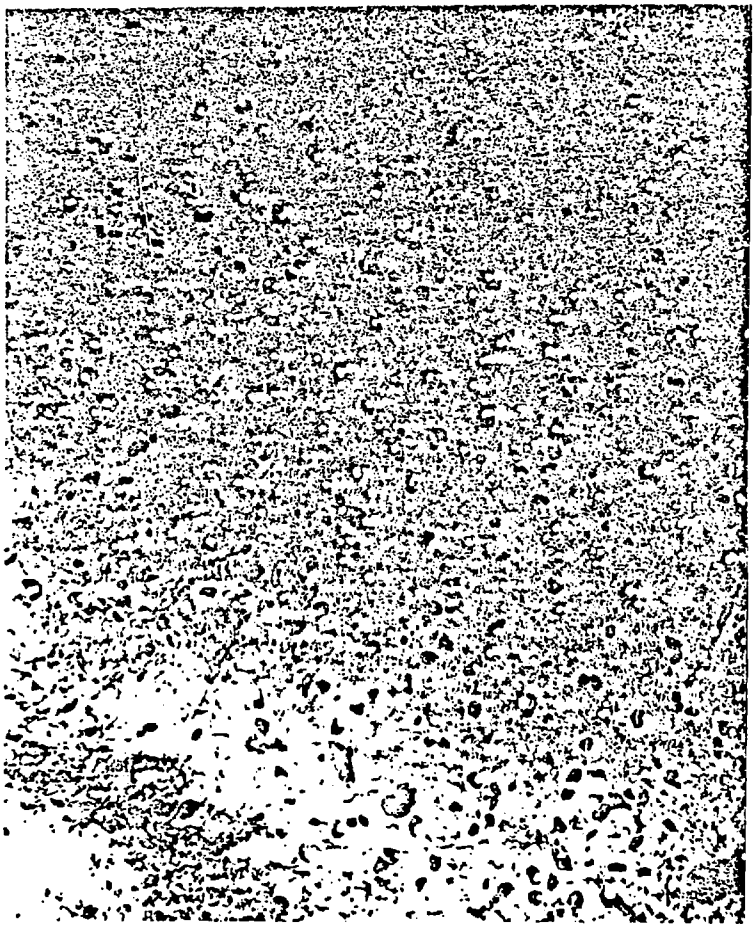

(a)

F.3

(a)

(b)

(c)

(d)

ORNL-DWG 86-8983

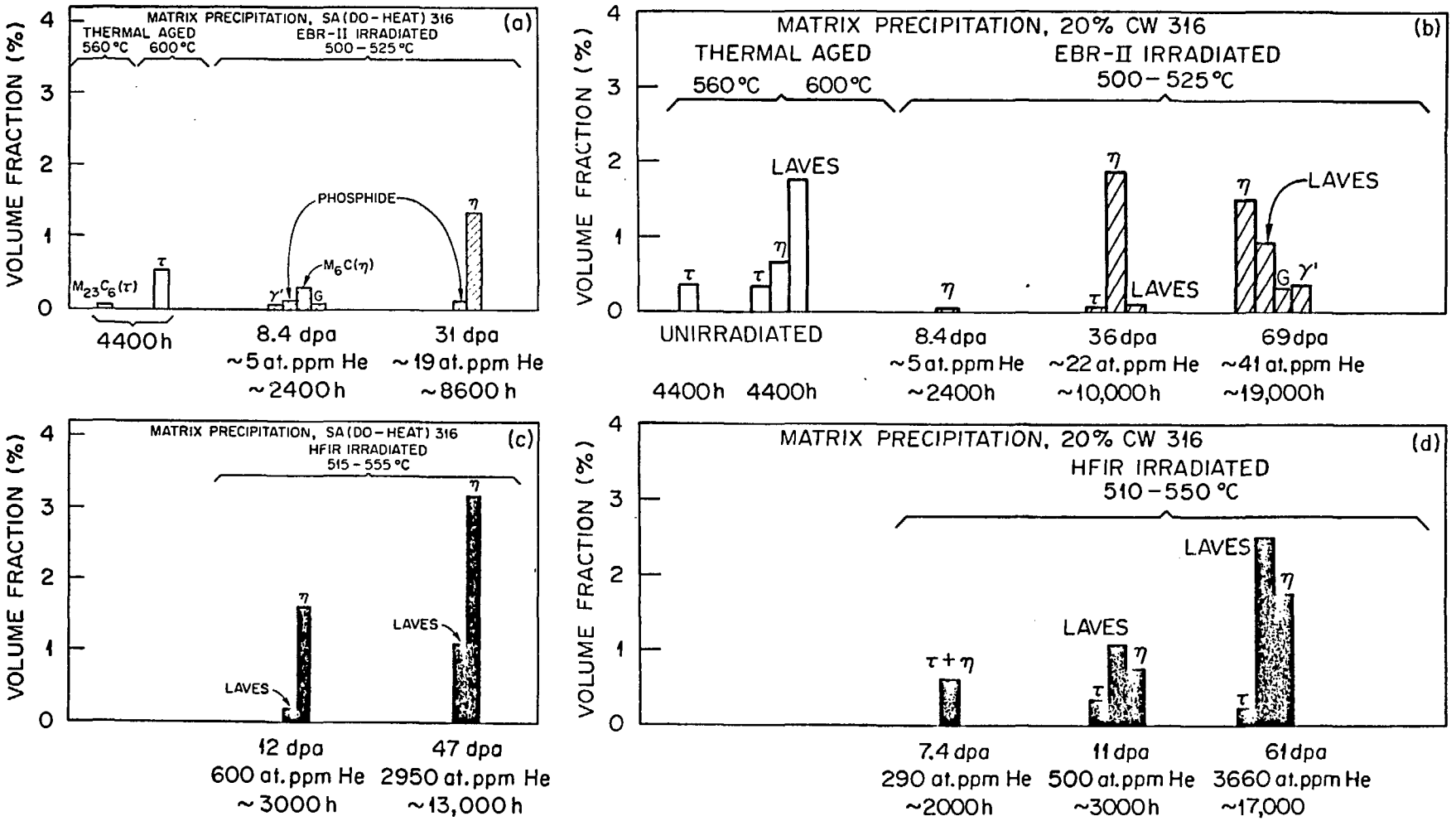

ORNL-DWG 85-17866R

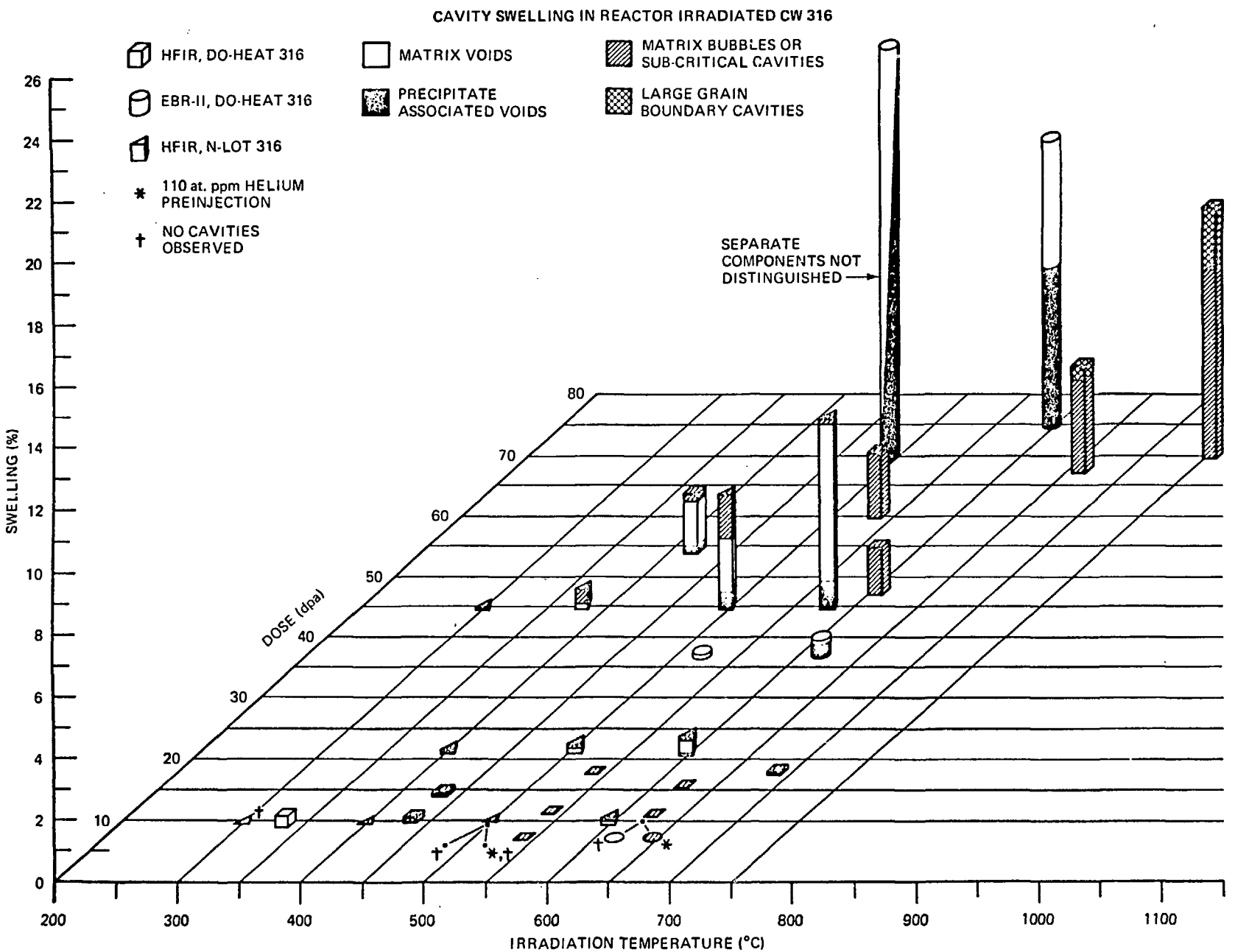

(a)

(b)

(c)

(d)

(e)

(f)

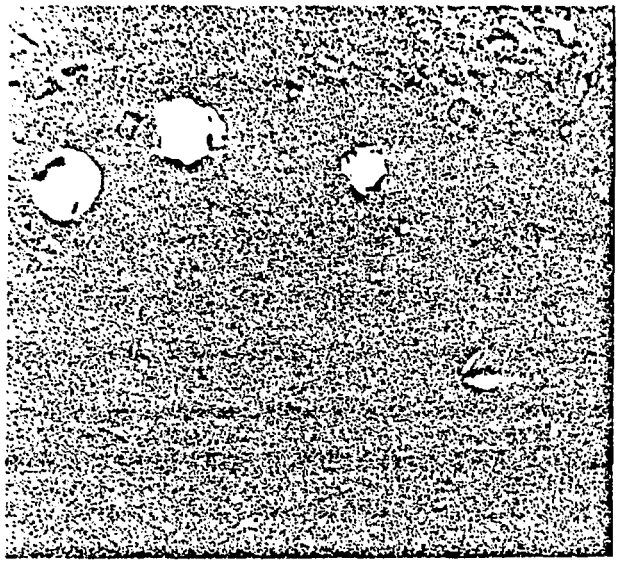

(a)

(b)

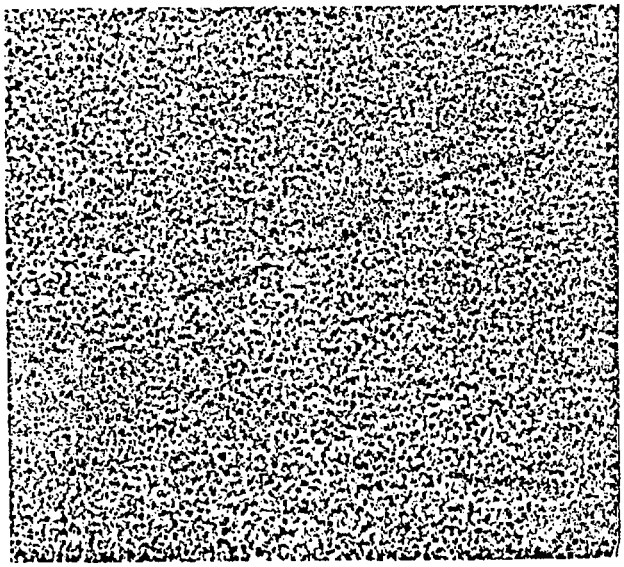

(c)

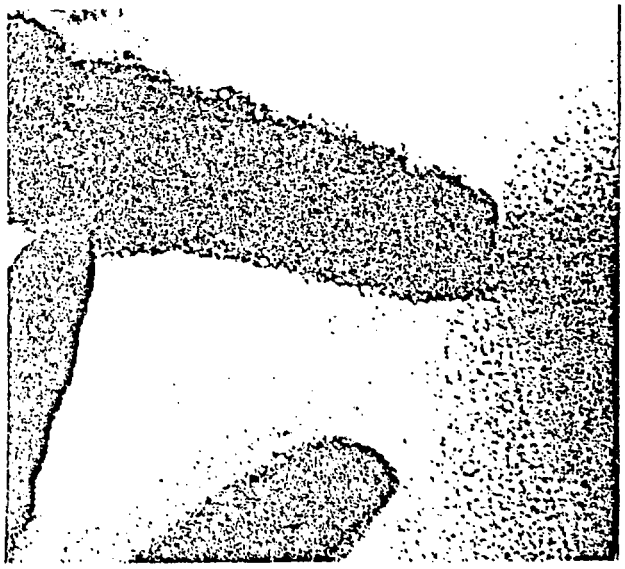

(d)

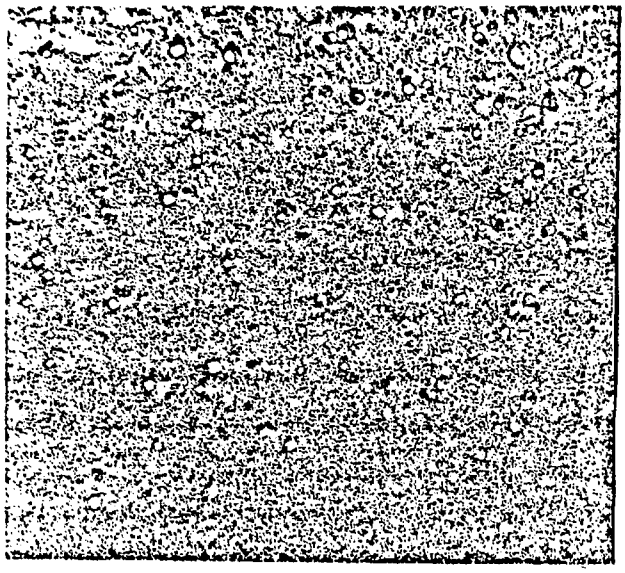

(a)

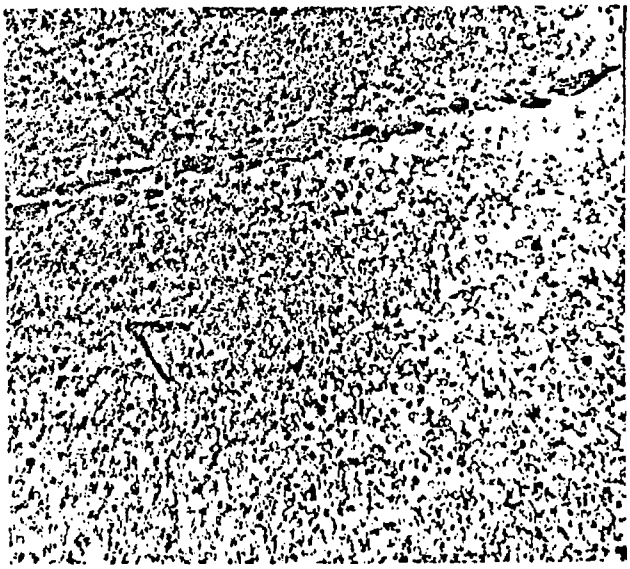

(c)

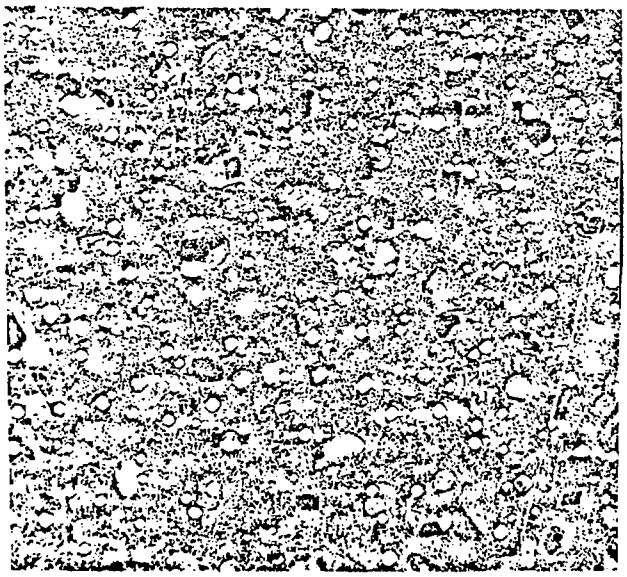

(b)

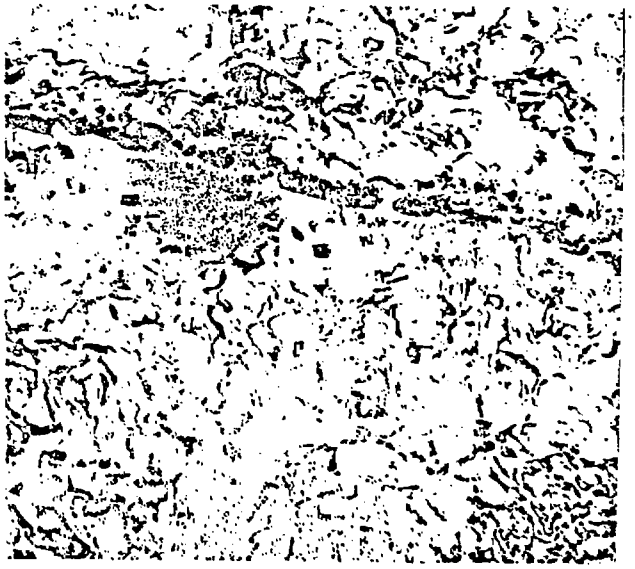

(d)

(c)

(b)

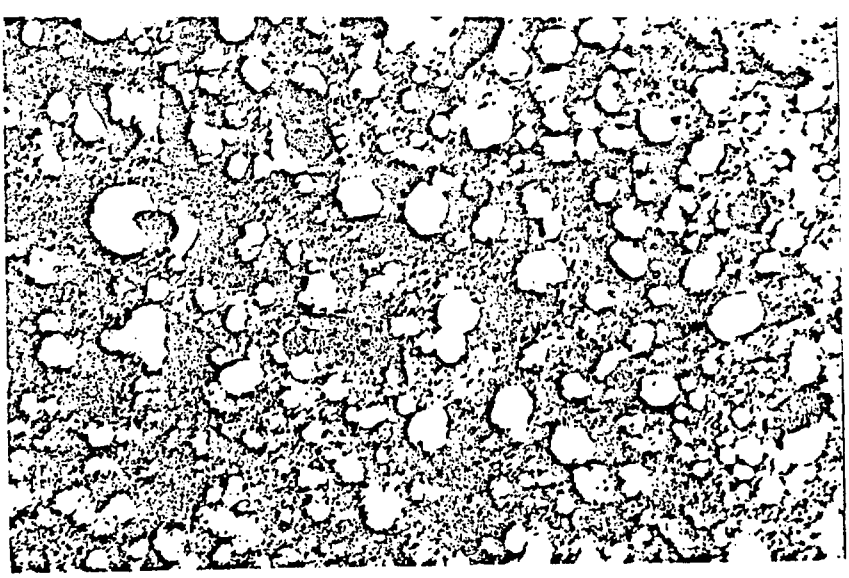

(a)

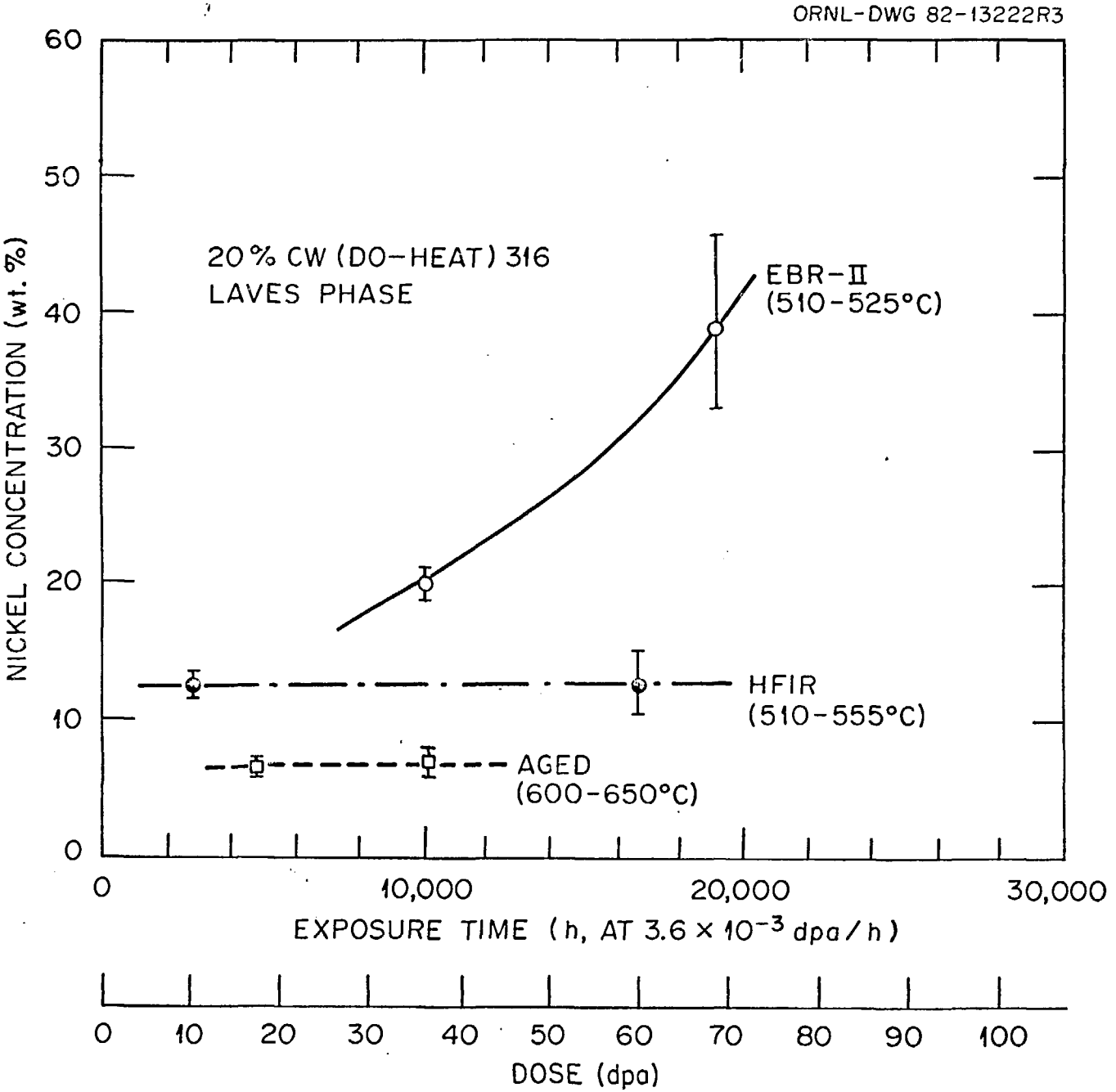
ORNL-DWG 82-13222R3
NICKEL CONCENTRATION (wt. %)
60
50
40
30
20
10
0
20% CW (DO-HEAT) 316
LAVES PHASE
EBR-II
(510-525°C)
HFIR
(510-555°C)
AGED
(600-650°C)
0
10,000
20,000
30,000
EXPOSURE TIME (h, AT 3.6 × 10⁻³ dpa/h)
0
10
20
30
40
50
60
70
80
90
100
DOSE (dpa)

(a)

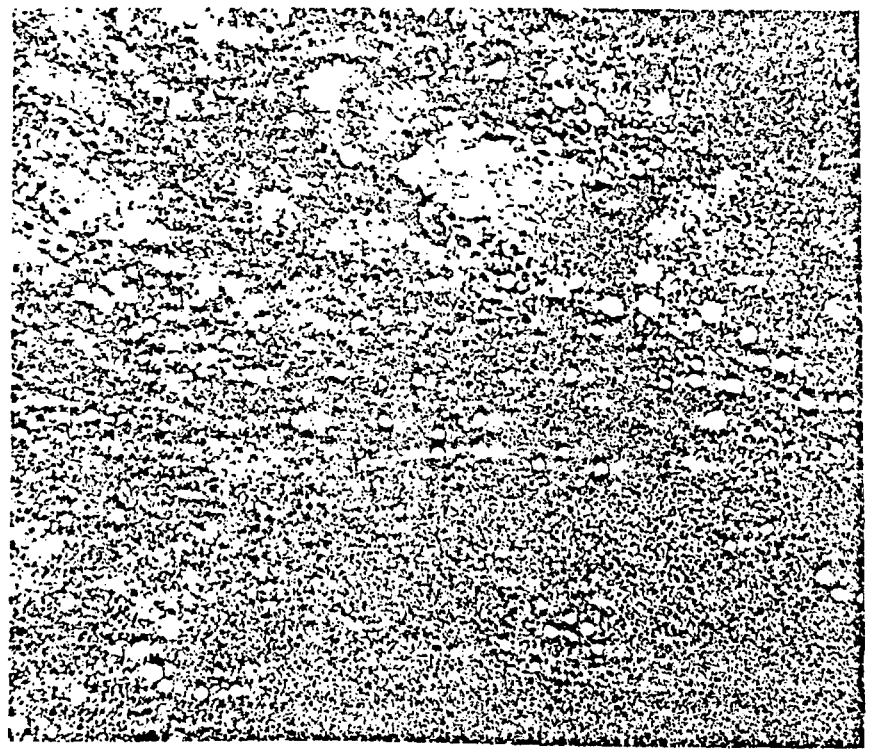

(b)

Table 1. Composition of two heats of type 316 stainless steel

Heat Designation	Alloy Composition, wt. %												
	Fe	Cr	Ni	Mo	Mn	Si	C	Ti	P	S	N	B	Co
DO-heat 316	Bal	18.0	13.0	2.6	1.9	0.8	0.05	0.05	0.01	0.016	0.05	0.0005	0.004
N-lot 316	Bal	16.5	13.5	2.5	1.6	0.5	0.05		0.01	0.006	0.006	0.0008	0.05

Table 2. Microstructural evolution in EBR-II irradiated SA (DO-heat) 316 austenitic stainless steel

Temperature [°C]	Dose [dpa]	Swelling[a] [%]	Matrix bubbles $\bar{d}$[nm]; N[m^{-3}]	Matrix voids $\bar{d}$[nm]; N[m^{-3}]	Precipitate voids $\bar{d}$[nm]; N[m^{-3}]	Precipitate phases[b]	Dislocation density[c] [m/m^3]
500	8.4	0.05	--	--	52.7; 5.4×10^{18}	M_6C-$\eta(m)$ phosphides (i) G(i) Ni_3Si-γ'(i)	(F.L. + N) 7.8×10^{13}
525	31	0.27	1.8; 3.4×10^{21}	23; 2.5×10^{19}	56; 1.8×10^{19}	η(m) phosphides (i)	(N) 1.9×10^{14}
625	8.4	0.16	3; 6.7×10^{18}	--	57.6; 8.6×10^{19}	η(e) phosphides (i)	(F.L. + N) 5.7×10^{13}
630	36	1.5	4.8; 1.2×10^{20}	65; 2.8×10^{18}	166; 4.5×10^{18}	Laves (m)	(N) 2×10^{13}

[a]Swelling is total for all cavity components and calculated by integrating over cavity size distributions.

[b]The letters in parenthesis after each precipitate phase indicate: i: radiation induced; m: radiation modified; e: radiation enhanced; t: thermal phase. The phases are listed in order of decreasing relative abundance.

[c]N: Network, F.L.: Frank loops.

Table 3. Microstructural evolution in EBR-II irradiated 20% CW (DO-heat) 316 austenitic stainless steel

Temperature [°C]	Dose [dpa]	Swelling[a] [%]	Matrix bubbles $\bar{d}$[nm]; N[m^{-3}]	Matrix voids $\bar{d}$[nm]; N[m^{-3}]	Precipitate voids $\bar{d}$[nm]; N[m^{-3}]	Precipitate phases[b]	Dislocation density[c] [m/m^3]
500–530	8.4			--	--	M_6C-η(e)	(N) 3.4×10^{14}
	36	0.05	3; 7×10^{20}	60; 5×10^{18}[d]		η(e), Laves(m)	(N) 2×10^{14}
	69	13.3	16.2; 2.4×10^{18}	126; 9×10^{19}[d]		η(e), Laves(m) γ'(i), G(i)	(N) 2×10^{14}
600–630	8.4	--	--	--		Laves(t), η(t)	(N) 2×10^{14}
	36	0.5	5; 7.5×10^{20}	93.4; 5.4×10^{18}	146; 4.6×10^{18}	η(e), Laves (t) $M_{23}C_6$-τ(t)	(N) 1×10^{14}
	75	9	8–57 ; 4×10^{19}	141; 3×10^{19}	500; 7.4×10^{17}	Laves (m), η(m) τ(t), σ(t)	(N) 1×10^{14}

[a-c]See footnotes to Table 2.

[d]Matrix + ppt voids.

Table 4. Microstructural evolution in helium pre-injected (110 at. ppm) and EBR-II irradiated (90-heat) 316 austenitic stainless steel (Dose: 8.4 dpa)

Initial condition	Temperature [°C]	Swelling [%]	Matrix bubbles $\bar{d}$[nm]; N[m^{-3}]	Precipitate phases*	Dislocation density* [m/m^3]
SA	500	0.01	2.1; 2.1×10^{22}	--	(F.L.) 6.4×10^{13}
	625	0.01	2.8; 9.5×10^{21}	η(t), Laves (t)	(N) 3.4×10^{13}
20% CW	500	--	--	--	(N) 3×10^{14}
	625	0.1	3.9; 2.7×10^{22}	η(t), Laves (t)	(N) 3×10^{14}

*See footnotes (b) and (c) to Table 2.

Table 5. Microstructural evolution in HFIR irradiated SA (DO-heat) 316 austenitic stainless steel

Temperature [°C]	Dose[a] [dpa]	Swelling[b] [%]	Matrix bubbles $\bar{d}$[nm]; N[m^{-3}]	Matrix voids $\bar{d}$[nm]; N[m^{-3}]	Precipitate voids $\bar{d}$[nm]; N[m^{-3}]	Precipitate phases[c]	Dislocation density[d] [m/m^3]
325–350	5.3[180]	--	--	--	--	--	(F.L.) 3×10^{15}
425–450	9.2[380]	0.18	2.3; 1.4×10^{22}	13.5; 1.1×10^{21}		γ'(i) η(m)	(F.L. + N) 5×10^{14}
	14.3[780]	0.65	1.6; 1.1×10^{22}	21; 4.3×10^{20}	34.5; 1.4×10^{20}	γ'(i) η(m)	(F.L. + N) 2.7×10^{14}
515–555	12 [660]	0.09	(5.6; 5×10^{21})[e] (12.7; 2.4×10^{20})	--	--	η(m) Laves(m)	(N) 5.6×10^{13}
	17.8[1020]	0.2	(10.5; 1.5×10^{21})[e] (17.4; 3.6×10^{20})	--	--	η(m) Laves(m)	(N) 2×10^{13}
	47 [3000]	9.7	2.2; 2.7×10^{23}	35; 1×10^{21}	76; 3×10^{20}	η(m) Laves(m)	(N + F.L.) 4×10^{14}
615–640	10 [440]	0.07	18.7; 1.8×10^{20}	--	--	Laves(t), η(t), τ(t)	(N) 1.2×10^{13}
	16.6[880]	0.13	18.9; 3.2×10^{20}	--	--	Laves(t), η(t) τ(t), σ(t)	(N) 9×10^{12}
	47 [3000]	9.3	--	50; 4.5×10^{20}	335; 1.2×10^{18}	$\eta(\tau)$, Laves(t), τ(t)	(N) 1.6×10^{13}
625–650	33.5[2000]	2.0	60; 4.8×10^{20}	--	--	Laves(t), σ(t)	(N) 2.4×10^{13}
730–755	53 [3300]	1.7	39; 4.8×10^{20}	--	--	χ(t), σ(t)	(N) not measured
	68.5[4140]	7.3[f]	110; 4.6×10^{19}	--	--	σ(t)	(N) 3×10^{12}

[a]Numbers in brackets indicate total amount of produced helium in units of at. ppm.

[b-d]See footnotes to Table 2.

[e]Bimodal size distribution.

[f]3% of the swelling is due to large grain boundary bubbles.

Table 6. Microstructural evolution in HFIR irradiated 20% CW (DO-heat) 316 austenitic stainless steel

Temperature [°C]	Dose[a] [dpa]	Swelling[b] [%]	Matrix bubbles $\bar{d}$[nm]; N[m^{-3}]	Matrix voids $\bar{d}$[nm]; N[m^{-3}]	Precipitate voids $\bar{d}$[nm]; N[m^{-3}]	Precipitate phases[c]	Dislocation density[d] [m/m^3]
325–350	8.4[390]	0.5	--	12; 4×10^{21}	--	--	(F.L. + N) 6×10^{14}
425–455	9.2[380]	0.12	2.7; 2×10^{22}	7.6; 2×10^{21}	--	γ'(i)	(F.L. + N) 1.5×10^{15}
	14.3[740]	0.03	2.6; 2×10^{23}	--	--	η(m)	(N) 2.5×10^{14}
	55 [3320]	2.0	5.3; 2.5×10^{22}	20; 2.6×10^{21}	70; 7.4×10^{18}	η(m)	(N) not measured
525–550	7.4[290]	0.01	2.6; 8.4×10^{21}	--	--	η(e), τ(e)	(N) 4×10^{14}
	10.9[500]	0.06	7; 2.6×10^{21}	--	--	Laves(e), η(e), τ(e)	(N) 1×10^{14}
	17.8[1020]	0.02	2.2; 2×10^{22}	--	--	Laves(e), η(e), τ(e)	(N) 1.5×10^{14}
	61 [3660]	2.0	17; 6.6×10^{21}	--	--	Laves e, η(e), τ(e)	(N) not measured
615–640	10 [440]	0.06	11; 5.6×10^{20}	--	--	Laves(t), τ(t), η(t)	(N) 1×10^{14}
	16.6[880]	0.15	22; 2.7×10^{20}	--	--	Laves (t), τ(t), η(t), σ(e)	(N) 8×10^{13}
	47 [3000]	1.4	21; 2.4×10^{21}	--	--	Laves(t), η(t), τ(t), σ(e)	(N) not measured
650–700	17.8[1020]	0.14	21.5; 2×10^{20}	--	--	τ(e), σ(e) Laves(t), x(e)	(N) 4×10^{12}
	67 [4070]	3.4	65; 3.3×10^{20}	--	--	τ(e), σ(e) x(e)	(N) $<1 \times 10^{12}$
730–755	69 [4140]	8.0[e]	110; 6.5×10^{19}	--	--	σ(e), x(e)	(N) $1\text{-}3 \times 10^{12}$

[a-d] See footnotes to Table 5.
[e] 2% of the swelling is due to large grain boundary bubbles.

Table 7. Microstructural evolution in HFIR irradiated 20% cw (N-lot) 316 austenitic stainless steel

Temperature [°C]	Dose [dpa]	Swelling[a] [%]	Matrix bubbles $\bar{d}$[nm]; N[m^{-3}]	Matrix voids $\bar{d}$[nm]; N[m^{-3}]	Precipitate voids $\bar{d}$[nm]; N[m^{-3}]	Precipitate phases[b]	Dislocation density[c] [m/m^3]
300	10[375]	--	--	--	--	--	
	44[3000]	0.1	2.3; 1.6×10^{23}	--	--	--	F.L. (*many*)
400	10[440]	0.06	3.2; 3.7×10^{22}[d]	--	--	--	(F.L. + N)
	22[1440]	0.14	3.2; 7.4×10^{22}[d] 5.4; 1.6×10^{21}[d]	--	--	VC-?(e)	(F.L. + N)
	44[3000]	0.7	4; 1.2×10^{23}	6.4; 7.3×10^{21}	15.4; 1.8×10^{20}		(F.L. + N) $>2 \times 10^{14}$
500	10[440]	0.05	2.1; 3.5×10^{22}[d] 4.5; 3×10^{21}[d]	--	--	γ'(i)	(F.L. + N)
	22[1440]	0.15	4; 3.7×10^{22}	10; 1.7×10^{21}	--	η(e), γ'(i)	(F.L. + N)
	44[3000]	3.6	5.8; 7.2×10^{22}	13.3; 1×10^{22}	60; 1.7×10^{19}	η(e)	(F.L. + N) $>2 \times 10^{14}$
600	10[470]	0.2	3.2; 2.5×10^{22}	10; 1.1×10^{21}	--	γ'(i), η(e)	(F.L. + N)
	22[1470]	>0.5	4.5; 2.2×10^{22}	12; 3×10^{21}	20-50[e]	η(e), γ'(i)	(F.L. + N)
	44[3000]	6	9.3; 2.5×10^{21}	30; 2.7×10^{21}	86; 1.9×10^{19}	η(e)	(N) $<2 \times 10^{14}$

[a-d]See footnotes to Table 5.

[e]Voids attached to coarse η particles heterogeneously formed along faulted bands; N not measured.

TABLE IX
CORRELATION OF PHASE NATURE AND VOID ASSOCIATION CHARACTERISTICS IN NEUTRON IRRADIATED TYPE 316 (DO-HEAT) STAINLESS STEEL

PHASE	CRYSTAL STRUCTURE[a] AND LATTICE PARAMETER[b]	VOLUME MISFIT[c]	VOID ASSOCIATION UNDER IRRADIATION: COMMENTS	VOID ASSOCIATION UNDER IRRADIATION: PHASE COMPOSITION[d]	THERMAL PHASE BEHAVIOR: COMMENTS	THERMAL PHASE BEHAVIOR: PHASE COMPOSITION
M_6C(η)	CUBIC, Fd3m, $E9_3$ (a_0 = 1.08 nm)	0.1	VOIDS ATTACHED UNDER A VARIETY OF CONDITIONS. RADIATION *ENHANCED OR* MODIFIED.	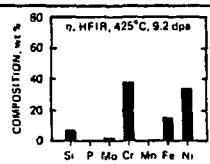	*FORMS IN CW AND* SA 316 FROM 600–700°C AFTER 2770–10,000h.	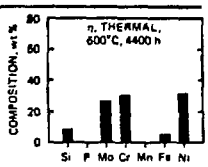
LAVES	HEXAGONAL, $P6_3/mmc$, C14 (a_0 = 0.47 nm, a_0/c_0 = 0.77)	~0.05	VOIDS ATTACHED UNDER A VARIETY *OF CONDITIONS.* RADIATION ENHANCED OR MODIFIED.	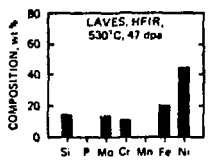	FORMS IN CW AND SA 316 FROM 600–800°C AFTER 2770–10,000h.	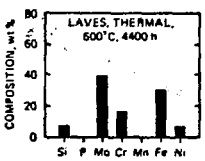
A-PHOSPHIDES: Fe_3P TYPE,[e] HEXAGONAL, P321, C22 (a_0 = 0.6 nm, c_0/a_0 = 0.6)		~0.4	VOIDS ATTACHED TO MANY, BUT NOT ALL PARTICLES. RADIATION INDUCED.	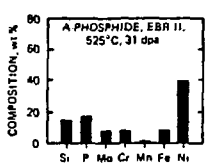	NOT FORMED IN TYPE 316	
AND/OR						
B PHOSPHIDES: Cr_3P TYPE, TETRAGONAL, I4, $S2_1^2$ (a_0 = 0.92 nm, c_0/a_0 = 0.5)		~0	VOIDS ATTACHED TO SOME, BUT NOT ALL PARTICLES. RADIATION INDUCED.	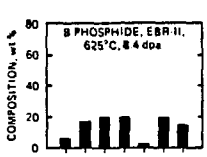	NOT FORMED IN TYPE 316	
G-PHASE	CUBIC, Fm3m, A1 (a_0 = 1.1 nm)	0.05	VOIDS ATTACHED TO NEARLY ALL PARTICLES. *RADIATION INDUCED.*	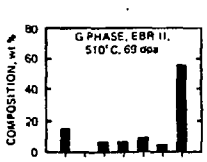	NOT FORMED IN TYPE 316	
Ni_3Si(γ')	CUBIC, P3m3, $L1_2$ (a_0 = 0.35 nm)	~0.1	VOIDS ARE NOT ATTACHED RADIATION INOUCED.	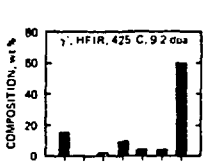	NOT FORMED IN TYPE 316	
$M_{23}C_6$(τ)	CUBIC, Fm3m, $D8_4$ (a_0 = 1.06 nm)	0.1	VOIDS ARE NOT ATTACHED RADIATION RETARDED PHASE UNDER MOST CONDITION, BUT FORMS IF RIS IS *SUPPRESSED.*		FORMS IN CW AND SA 316 FROM 560–800°C AFTER 100–10,000h	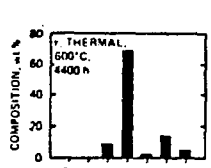
σ	TETRAGONAL, $P4_2/mnm$, $D8_b$ (a_0 = 0.88 nm, c_0/a_0 = 0.52)	~0	VOIDS ARE NOT ATTACHED. RADIATION RETAROED PHASE UNDER MOST CONDITIONS, *BUT FORMS ABOVE 600°C IF RIS* IS SUPPRESSED.		*FORMS IN CW* AND SA 316 FROM 650–900°C AFTER 2770–10,000h.	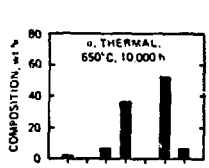

[a] FOR EACH PHASE (LATTICE SYSTEM, SPACE GROUP, STRUCTURE TYPE) WHERE LATTICE SYSTEMS IS THE BRAVAIS LATTICE TYPE – SPACE GROUP IS GIVEN BY THE SHORT FORM OF THE POINT GROUP SYMMETRY ELEMENTS IN THE HERMANN MAUGUIN SHORT NOTATION. STRUCTURE TYPES IS THE STRUKTURBERICHT NOTATION FOR THE ELEMENT OR PURE COMPOUND THAT IS THE *PROTOTYPE STRUCTURE FOR* THAT CRYSTAL CLASS. C. J. SMITHELLS, ED., *METALS REFERENCE BOOK*, 5th ED., BUTTERWORTHS, LONDON, 1976, pp. 108–77.

[b] E. H. LEE, P. J. MAZIASZ, AND A. F. ROWCLIFFE, "THE STRUCTURE AND COMPOSITION OF PHASES OCCURRING IN AUSTENITIC STAINLESS STEELS IN THERMAL AND IRRADIATION ENVIRONMENTS," pp. 191–218 IN CONF. PROC. *PHASE STABILITY DURING IRRADIATION*, EDS. J. R. HOLLAND, L. K. MANSUR, AND D. I. POTTER, THE METALLURGICAL SOCIETY OF AIME, WARRENDALE, PA. (1981).

[c] FRACTIONAL DIFFERENCE BETWEEN VOLUME PER SOLUTE ATOM IN NEW *PHASE COMPARED TO ORIGINAL AUSTENITE*

[d] PHASE COMPOSITION MEASURED BY X-RAY ENERGY DISPERSIVE SPECTROSCOPY FROM EXTRACTION REPLICA PRODUCED FROM EITHER SA OR CW (DO HEAT) 316 IRRADIATED TO THE *CONDITIONS INDICATED*. THE PARTICULAR PHASE COMPOSITION WAS SELECTED FROM IRRADIATION CONDITIONS PRODUCING EITHER MAXIMUM VOID ASSOCIATION WITH THAT PHASE AND OR MAXIMUM RADIATION INDUCED SOLUTE SEGREGATION (RIS).

[e] IDENTIFICATION WORK IS DIFFICULT AND STILL INCOMPLETE AS TO WHICH PHOSPHIDE (A OR B) IS Fe_3P OR Cr_3P